Comparison of pixel unmixing models in the evaluation of post-fire forest resilience based on temporal series of satellite imagery at moderate and very high spatial resolution

José Manuel Fernández-Guisuraga [a],[*], Leonor Calvo [a], Susana Suárez-Seoane [b],[c]

[a] Biodiversity and Environmental Management Dpt., Faculty of Biological and Environmental Sciences, University of León, 24071 León, Spain
[b] Organisms and Systems Biology Dpt., Faculty of Biology, University of Oviedo, 33071 Oviedo, Spain
[c] Research Unit of Biodiversity (UO, CSIC, PA), University of Oviedo, 33600 Mieres, Spain

ARTICLE INFO

ABSTRACT

In Mediterranean fire-prone ecosystems, shifts in fire regime as a consequence of global change could modify the resilience of vegetation communities. In this paper, we aim to compare the efficiency of high and moderate spatial resolution satellite imagery in the evaluation of resilience in a fire-prone landscape under different fire regime categories using two pixel unmixing techniques. A time series of Landsat (ETM+ and OLI; spatial resolution of 30 m) and WorldView-2 (spatial resolution of 2 m) imagery collected between 2011 (pre-fire conditions) and 2016 were used to estimate the temporal variation of fractional vegetation cover (FVC) as a quantitative measure of forest resilience. For this time series, FVC was computed under four fire-regime categories of recurrence and severity using two approaches: dimidiate pixel model and multiple endmember spectral mixture analysis (MESMA). The dimidiate pixel model was computed using NDVI as spectral response for the case of Landsat imagery and NDVI and red-edge NDVI (RENDVI) for WorldView-2. MESMA was applied to unmix WorldView-2 and Landsat imagery into four fraction images: photosynthetic vegetation (PV), non-photosynthetic vegetation (NPV), soil and shade. The PV shade normalized fraction corresponds to the FVC. In summer of 2016 we established 85 30 × 30 m field plots and 360 2 × 2 m field plots to measure the percentage of total vegetation cover in order to validate the FVC estimates made from remote sensing data. The FVC time series showed the same general pattern with both spatial scales and modeling approaches, high fire recurrence categories registering the highest resilience. The accuracy of the dimidiate pixel model was significantly higher for WorldView-2 based estimates (RMSE: 5–10%) than for Landsat (RMSE: 10–15%). The dimidiate pixel model computed from NDVI for both Landsat and WorldView-2 underestimated FVC at high field-sampled vegetation cover, while MESMA estimations were accurate for the entire range of vegetation cover for both satellites. The fraction of photosynthetic vegetation calculated using WorldView-2 had a higher performance (RMSE: 4–6%) than that quantified from Landsat (RMSE: 6–8%). The linear relationships assumed for validation purposes were statistically significant for both sensors and modeling approaches. Our study demonstrates the highest performance of very high spatial resolution satellite imagery and MESMA models in the quantitative estimation of FVC as a measure of post-fire resilience.

1. Introduction

Climatic and socioeconomic changes mainly occurred since the second half of the last century (Doblas-Miranda et al., 2017; Vilà-Cabrera et al., 2018) are major drivers that have led to an increase in the extent, recurrence and severity of wildfires in fire-prone ecosystems in the Mediterranean Basin (Chuvieco et al., 2010; Álvarez et al., 2012; Pausas and Fernández-Muñoz, 2012; Quintano et al., 2015; Fernández-García et al., 2018a). In these ecosystems,

shifts in fire regime can modify the resilience of vegetation communities (Doblas-Miranda et al., 2017), depending mainly on species adaptive traits (i.e. resprouting from parental tissues and seedling recruitment) (e.g. Pausas and Keeley, 2014; Tessler et al., 2014; González-De Vega et al., 2016).

In European Mediterranean areas, fire-prone pine ecosystems, such as those dominated by *Pinus pinaster* Aiton, are particularly subject to the occurrence of wildfires (Fernández-García et al., 2018a). High fire recurrence and burn severity in these ecosystems may jeopar-

dize forest resilience as the result of both a decrease in the resprouting capacity of vegetation (Díaz-Delgado et al., 2002; Doblas-Miranda et al., 2017) and a failure of seedling recruitment in short interval between fires (Calvo et al., 2008; Calvo et al., 2016; Doblas-Miranda et al., 2017). Therefore, the assessment of how forest evolves towards its pre-fire structure and function should be conducted considering the spatial variation of fire regime parameters. This evaluation is essential for understanding the impact of wildland fires in the ecosystems, as well as for endorsing post-fire management decision-making (De Santis and Chuvieco, 2009; Veraverbeke et al., 2012).

Fractional vegetation cover (FVC) is a canopy biophysical property (Gitelson et al., 2002) that can be used to measure quantitatively ecosystem resilience because it characterizes vegetation quality and reflects ecosystem changes (Jiapaer et al., 2011; Chu et al., 2016; Wang et al., 2017; Gao et al., 2020). This parameter is defined as the ratio of vertical projected area of green vegetation to the total statistical area of land surface (Gitelson et al., 2002; Li et al., 2015a, 2015b; Song et al., 2017). The traditional method for measuring FVC is based on field surveys (Li et al., 2015a, 2015b). This method presents high reliability (Zhang et al., 2013), but is expensive, labor-intensive and time-consuming (Liang et al., 2008; Veraverbeke et al., 2012; Fernandez-Manso et al., 2019), so its wide scale application is unfeasible (Jia et al., 2015). Nowadays, remote sensing techniques (RST) are recognized as the most efficient way to derive FVC on a large scale (Song et al., 2017). However, accurate ground measures of FVC are indispensable for remote sensing data validation (White et al., 2000; Zhou and Robson, 2001). Conventionally, low spatial resolution satellite sensors (e.g. NOAA-AVHRR, MODIS and HJ-1/HSI) (Gutman and Ignalov, 1998; DeFries et al., 1999; Zeng et al., 2000; Scanlon et al., 2002; Montandon and Small, 2008; Okin et al., 2013; Zhang et al., 2013; Jia et al., 2015) and moderate spatial resolution satellite sensors (e.g. Landsat and AVIRIS) (Roberts et al., 1998; Jiapaer et al., 2011; Delamater et al., 2012; Veraverbeke et al., 2012; Chu et al., 2016) have been used to estimate FVC. Nevertheless, the spatial resolution of these sensors is commonly larger than the length scale of heterogeneous landscapes (Garrigues et al., 2008; Li et al., 2015a, 2015b), probably containing a single pixel spectra from different ground covers (Xiao and Moody, 2005). Moreover, FVC field validation requires information on the scale of individual plant elements, this approach being problematic with coarse satellite imagery (Gutman and Ignalov, 1998). Hence, high spatial resolution satellite imagery could be more suited for the accurate monitoring of post-fire resilience in heterogeneous landscapes, where the vegetation horizontal structure varies at fine scale (Meng et al., 2017; Meng et al., 2018).

Several approaches can be used to estimate FVC from remote sensing techniques as a measure of post-fire resilience: empirical, pixel unmixing and physical-based models. (i) Empirical models have been used in numerous studies (Graetz et al., 1988; Dymond et al., 1992; Wittich and Hansing, 1995; Purevdor et al., 1998; North, 2002; Cuevas-González et al., 2009; Hill et al., 2017), but this approach is highly dependent on local measurements (Jiapaer et al., 2011) and an exhaustive transferability analysis is required for its application on large spatial scales (Fernández-Guisuraga et al., 2019a). (ii) Pixel unmixing models rely on the assumption that the image pixel consists of several spectrally distinct ground components that contribute a part to the surface reflectance captured by the remote sensor (Zhang et al., 2013; Li et al., 2015a, 2015b), being the pixel FVC the ground component proportion that corresponds to vegetation cover (Wang et al., 2017). In this approach, ground cover abundance is directly derived from remote sensing data, without the need of an initial calibration based on field data (Veraverbeke et al., 2012). Among the existing pixel unmixing models, the dimidiate pixel model assumes that pixel spectral information is a linear combination of only two components: vegetation and non-vegetation cover (Jiapaer et al., 2011; Wang et al., 2017). This model has been successfully used

in several studies to estimate FVC (Gutman and Ignalov, 1998; Wu et al., 2004; Jiang et al., 2006; Montandon and Small, 2008; Jing et al., 2010; Jiapaer et al., 2011; Johnson et al., 2012; Chu et al., 2016; Wei et al., 2018) and it is widely applicable at global scale without geographical constraints (Zhang et al., 2013). The main shortcoming of the dimidiate pixel model is the influence of background spectra variability in the FVC estimation (Montandon and Small, 2008; Ding et al., 2016) derived from the model assumption itself. The most common pixel unmixing approach is the linear spectral mixture analysis (LSMA) model to derive FVC from the spectral features of the ground components or endmembers (Xiao and Moody, 2005; Sankey et al., 2008; Jiménez-Muñoz et al., 2009; Solans-Vila and Barbosa, 2010; Jiapaer et al., 2011; Li et al., 2015a, 2015b). LSMA has a direct physical sense (Bian et al., 2016; Melville et al., 2019) and it is sensitive to small changes in the FVC (Elmore et al., 2000). However, only one spectral signature can be incorporated in each endmember to account for the variability of a terrain feature (Veraverbeke et al., 2012). In contrast, multiple endmember spectral mixture analysis (MESMA; Roberts et al., 1998) allows several endmember spectra to characterize each pixel constituting feature (Quintano et al., 2017) accounting for the natural variability of the ground feature (Veraverbeke et al., 2012). (iii) Finally, physical-based methods based on the inversion of radiative transfer models (RTMs) to simulate physical relationships between remote sensing data and FVC (Wang et al., 2017) have a sound theoretical basis but they are complex and the direct inversion is complicated (Jia et al., 2015). RTMs encompass leaf optical models (e.g. PROSPECT; Jacquemoud and Baret, 1990) used to simulate leaf reflectance and transmittance based on the leaf biochemical and anatomical properties (De Santis et al., 2009; Verrelst et al., 2016), canopy optical models (e.g. GeoSail; Huemmrich, 2001) used to simulate canopy reflectance and transmittance based on the canopy structural attributes (Kattenborn and Schmidtlein, 2019; Sinha et al., 2020), as well as coupled leaf-canopy models as PROSAIL (Jacquemoud et al., 2009) or PROSPECT + GeoSail (De Santis et al., 2009). In particular, the use of geometric canopy models such as GeoSail, coupled with a leaf model, allows the simulation of several vegetation layers for retrieving vegetation biophysical parameters in landscapes with structurally heterogeneous vegetation (Kötz et al., 2004; De Santis et al., 2009; Jurdao et al., 2013). Typically, the indirect inversion of RTMs using neural networks is one of the most widely used methods given its good computational efficiency and performance (Kallel et al., 2007; Jia et al., 2016). Therefore, this method is usually selected for FVC estimation at global scale (Verger et al., 2011; Baret et al., 2013; Yang et al., 2016). However, model inversion to retrieve vegetation biophysical variables has several uncertainties related to the lack of information on model parameters for particular regions, so the parameters are allowed to fluctuate between a certain range (Yebra and Chuvieco, 2009), as well as related to model simplifications concerning, for example, leaf scattering (Atzberger, 2004).

As noted above, most research addresses the FVC estimation using moderate or low spatial satellite imagery through any of the described approaches. High spatial resolution satellite imagery has received little attention for this purpose, especially in the fire ecology field, and is normally used to validate coarse resolution FVC data, to derive homogeneous endmembers to unmix coarse imagery or in image classification schemes (Melville et al., 2019). The increasing accessibility of high spatial resolution satellite imagery provides an opportunity to estimate post-fire FVC at fine scale in the assessment of the resilience of fire-prone ecosystems. Another knowledge gap is to determine which method of FVC quantitative estimation is the most appropriate in post-fire resilience studies at short-term.

The objective of this research paper was to compare the potentiality of satellite imagery at high and moderate spatial resolution in the evaluation of post-fire resilience in a Mediterranean fire-prone ecosystem. Specifically, we tried to: (1) Compare the efficiency of WorldView-

2 imagery and Landsat (ETM + and OLI) for the quantitative estimation of fractional vegetation cover for a time series in different post-fire recurrence and severity categories. (2) Evaluate the performance of different model approaches (dimidiate pixel model from different vegetation indices and multiple endmember spectral mixture analysis) for quantifying fractional vegetation cover as a measure of post-fire resilience with high and moderate spatial resolution imagery.

2. Materials and methods

2.1. Study area. Fire recurrence and severity

The study was conducted within the perimeter of a convective crown stand-replacing megafire that burned 11,602 ha of a forest dominated by *Pinus pinaster* in August 2012. The study area (Fig. 1) is located in northwest Spain (Sierra del Teleno mountain range), with an altitude between 836 and 1499 m a.s.l. This area presents an annual average rainfall and temperature of 640 mm and 10 °C (Ninyerola et al., 2005), respectively, with less than two months of summer drought. These climatic conditions correspond to a Mediterranean transition area (Fernández-Guisuraga et al., 2019b). The pre-fire landscape was dominated by mature *Pinus pinaster*, *Quercus pyrenaica* and *Quercus ilex* stands with a tall understory layer (Taboada et al., 2018). Vegetation following fire is dominated by tree regeneration stands in a seedling growth stage, with a shrubby understory layer dominated by *Halimium alyssoides*, *Pterospartum tridentatum* and *Erica australis* (Fernández-Guisuraga et al., 2019a). The study area is characterized by a strong environmental heterogeneity derived from the vegetation community structure and composition (Quintano et al., 2017; Fernández-Guisuraga et al., 2019b).

Considering the last 15 years, this area suffered another megafire in 1998 that burned 3000 ha. Therefore, we defined two fire recurrence categories: low fire recurrence (one fire in the last 15 years within the burnt scar of the 2012 fire) and high fire recurrence (two fires in the last 15 years within the burnt scar of the 2012 fire). Moreover, we estimated fire severity on the basis of the differenced Normalized Burn Ratio index (dNBR) (Key, 2006) derived from Landsat 7 ETM + pre-fire and post-fire images (September 20th, 2011 - September 6th, 2012) and the Composite Burn Index (CBI) (Key and Benson, 2006). CBI was measured three months after the fire over 54 field plots of 30 × 30 m randomly distributed across the study area, using an adapted version by Fernández-García et al. (2018b) of the original CBI protocol. We established two fire severity categories computed from CBI thresholds (Quintano et al., 2015) using a linear regression model: low severity (dNBR ≤ 573) and high severity (dNBR > 573) (Fig. 1). The correlation between dNBR and CBI had a coefficient of determination of 0.84.

2.2. Satellite imagery data and processing

Four images of Landsat (ETM + and OLI) and WorldView-2 sensors were acquired in summer months between 2011 (pre-fire conditions) and 2016 (Table 1) during peak biomass of the study area. Acquisition dates were chosen on the basis of the availability of the on-demand WorldView-2 imagery.

The Landsat imagery was downloaded from the USGS Earth Explorer server (http://earthexplorer.usgs.gov/) with a cloud cover lower than 5%. The spatial resolution of Landsat optical bands (ETM +: B1 to B5 and B7; OLI: B1 to B7) is 30 m and is delivered by the USGS geometrically rectified and radiometrically corrected (Fernández-García et al., 2018a). Landsat ETM + and OLI imagery were atmospherically and topographically corrected to a surface reflectance product using the ATCOR atmospheric correction algorithm (Richter and Schläpfer, 2018). Input data for the atmospheric correction (visibility and column water vapor amount) were acquired from the State Meteorology Agency of Spain (AEMET). Moreover, Landsat ETM + surface reflectance product was transformed with the statistical functions provided by Roy et al. (2016) to be comparable to Landsat OLI.

WorldView-2 imagery was delivered by DigitalGlobe with a spatial resolution of 2 m in the optical bands (B1 to B8) and a cloud cover lower than 10%. The imagery was orthorectified with rational polynomial coefficients (RPC) provided in the image metadata, a digital elevation model (DEM; RMSE_Z < 20 cm) and 100 ground control points. The atmospheric and topographic correction to obtain a surface reflectance product was similar to the procedure performed with Landsat imagery.

2.3. Derivation of FVC from a dimidiate pixel model using vegetation indices

In the dimidiate pixel model, FVC exhibits a linear relationship with the spectral response (S) of a mixed pixel representing vegetation -v- and soil -s- (Wittich and Hansing, 1995; Zhang et al., 2013) (Eq.
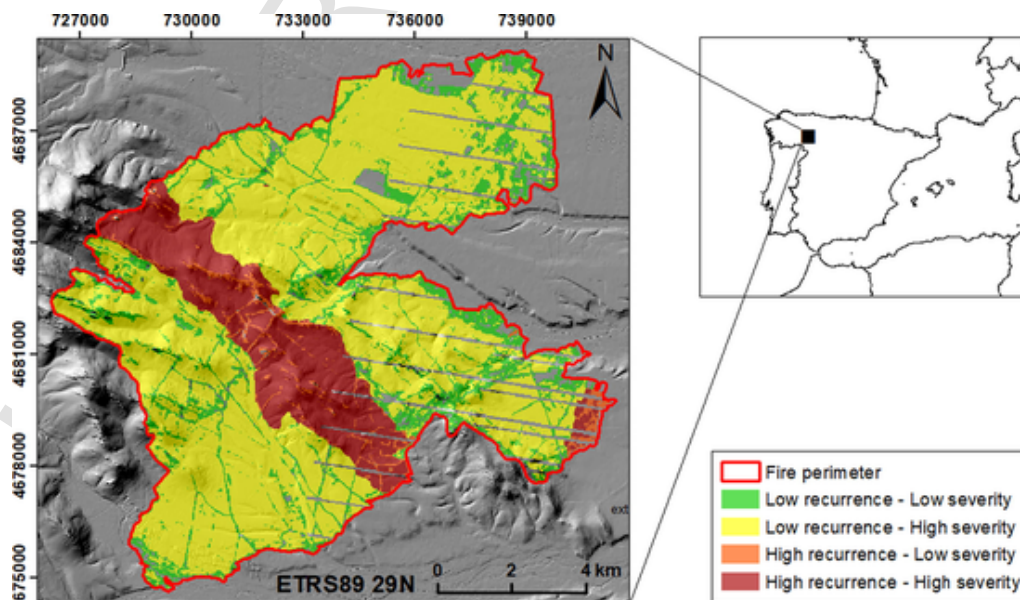

Fig. 1. Location of the study area within the burnt scar of 11,602 ha and recurrence-severity categories.

Table 1
Acquisition date of the satellite imagery used in the present study (Landsat ETM+ and OLI and WorldView-2) to assess fractional vegetation cover following fire.

Sensor	Acquisition date	Fire date equivalence
Landsat 7 ETM+	September 20, 2011	Pre-fire
WorldView-2	September 19, 2011	
Landsat 8 OLI	September 17, 2013	Year 1
WorldView-2	September 10, 2013	
Landsat 8 OLI	June 19, 2015	Year 3
WorldView-2	June 16, 2015	
Landsat 8 OLI	June 21, 2016	Year 4
WorldView-2	June 23, 2016	

(1)):

$$FVC = \frac{S - S_s}{S_v - S_s} \qquad (1)$$

In this approach, the most applied spectral response (S) for the estimation of FVC is the Normalized Difference Vegetation Index (NDVI) (Jiapaer et al., 2011; Yang et al., 2013; Zhang et al., 2013), which shows a high linear correlation with FVC (Zhang et al., 2013; Chu et al., 2016; Mu et al., 2018). Other authors suggested non-linear relationships (e.g. quadratic terms) (Carlson and Ripley, 1997; Gitelson et al., 2002), but they do not offer better results in all case studies (Wittich and Hansing, 1995; Jiménez-Muñoz et al., 2009).

We computed a time series of pre- and post-fire FVC in different categories of recurrence and severity by applying the dimidiate pixel model to Landsat (ETM+ and OLI) and WorldView-2 imagery, using NDVI as the spectral response for the former case and NDVI and red-edge NDVI (RENDVI; Xie et al., 2018) for the latter. The red-edge spectral region available in the WorldView-2 sensor has a great potential for the retrieval of vegetation biophysical variables (Xie et al., 2018) because of its high sensitivity to changes in the chlorophyll concentration of leaves and canopies, leaf area index and biomass density (Gitelson et al., 2005; Delegido et al., 2011). NDVI was calculated from Landsat ETM+ using the Eq. (2) and from Landsat OLI using the Eq. (3). In the case of WorldView-2, NDVI was computed with Eq. (4) and RENDVI with Eq. (5).

$$NDVI_{ETM+} = (B4 - B3) / (B4 + B3) \qquad (2)$$

$$NDVI_{OLI} = (B5 - B4) / (B5 + B4) \qquad (3)$$

$$NDVI_{WV-2} = (B7 - B5) / (B7 + B5) \qquad (4)$$

$$RENDVI_{WV-2} = (B7 - B6) / (B7 + B6) \qquad (5)$$

Introducing NDVI or REDNVI in Equation (1), FVC is estimated with Eq. (6):

$$FVC = \frac{(RE)NDVI - (RE)NDVI_s}{(RE)NDVI_v - (RE)NDVI_s} \qquad (6)$$

$(RE)NDVI_v$ and $(RE)NDVI_s$ parameters refer to representative $(RE)NDVI$ values for pure green vegetation pixel (FVC = 1) and for pure bare soil (FVC = 0), respectively. In some cases, the estimation of these parameters becomes challenging (Mu et al., 2018) because they are specific for each region and season (Jiménez-Muñoz et

al., 2009). The $(RE)NDVI_s$ value may change even in the same satellite scene depending on soil moisture and type (Zhang et al., 2013). In this paper, we used remote sensing data at very high spatial resolution (WorldView-2) and very high spatial resolution ortophotographs (0.5 m) provided by the Spanish National Center of Geographic Information (http://www.cnig.es/) to delineate training samples of pure green vegetation and bare soil, together with field knowledge. This is considered as an adequate method to estimate $(RE)NDVI_v$ and $(RE)NDVI_s$ parameters (Chu et al., 2016; Song et al., 2017). Training samples have enough size to accommodate at least a pure Landsat pixel within them. One hundred training samples of pure green vegetation and bare soil were delineated in the WorldView-2 image of each study year (2011, 2013, 2015 and 2016, i.e. pre-fire and one, three and four years after fire). For each year, the samples of pure green vegetation and bare soil were averaged to compute the $(RE)NDVI_v$ and $(RE)NDVI_s$ parameters, respectively, from Landsat and WorldView-2 imagery (Table 2).

2.4. Derivation of FVC from spectral mixture analysis

Multiple endmember spectral mixture analysis (MESMA) is an extension of linear spectral mixture analysis (LSMA) in which each pixel can be modeled with different numbers and types of endmembers (Roberts et al., 1998; Bue et al., 2015; Quintano et al., 2017). In this paper, the endmember spectra for MESMA were obtained from the imagery itself, instead of using spectral libraries, because: (i) image endmembers are collected at the same scale as the image data (Meng et al., 2017; Quintano et al., 2017); and, (ii) the ease of obtaining pure endmembers with fine-grained satellite imagery (Clark and Kilham, 2016; Meng et al., 2017). The first post-fire Landsat OLI and WorldView-2 images (one year after fire) were used to collect endmembers for each sensor because non-photosynthetic vegetation was not present in enough quantity in pre-fire and late (three and four years) post-fire imagery. Training areas consisting of uniform patches of a single ground cover type were defined in the first post-fire images to collect potential endmembers for each sensor. Training areas for soil (sandy soil -Soil 1- and red clay soil -Soil 2-), green vegetation (*Pinus pinaster*, *Quercus* sp. And shrub) and non- photosynthetic vegetation (woody debris and charred logs) were based on field knowledge and very high spatial resolution ortophotographs (0.5 m). Iterative end-

Table 2
Mean and standard deviation (std) of pure green vegetation and bare soil in the training samples to estimate the $(RE)NDVI_v$ and $(RE)NDVI_s$ parameters, respectively.

		Vegetation samples		
		WV-2 NDVI	WV-2 RENDVI	ETM+/OLI NDVI
2011	mean	0.8271	0.4324	0.7944
	std	0.0610	0.0312	0.1136
2013	mean	0.7722	0.4157	0.7668
	std	0.1278	0.0354	0.0742
2015	mean	0.8687	0.4357	0.7900
	std	0.0623	0.0367	0.0942
2016	mean	0.8311	0.3930	0.7951
	std	0.0806	0.0380	0.1114
		Soil samples		
		WV-2 NDVI	WV-2 RENDVI	ETM+/OLI NDVI
2011	mean	0.0730	0.0403	0.1258
	std	0.0224	0.0280	0.0452
2013	mean	0.0722	0.0422	0.1119
	std	0.0493	0.0264	0.0654
2015	mean	0.0676	0.0518	0.1173
	std	0.0321	0.0526	0.0507
2016	mean	0.0781	0.0429	0.1053
	std	0.0488	0.0447	0.0416

member selection (IES) (Schaaf et al., 2011; Roth et al., 2012) is a semi-automated technique that was used to select optimal endmembers from the spectral library and improve MESMA run times (Quintano et al., 2017). The selected endmembers were grouped into three spectral libraries: photosynthetic vegetation (PV), non-photosynthetic vegetation (NPV) and soil. Thus, the WorldView-2 and Landsat imagery were unmixed into four fraction images: PV, NPV, soil and shade. Following Roberts et al. (2003, 2012), Fernandez-Manso et al. (2016) and Quintano et al. (2017), the performance of all candidate models was assessed using the following criteria for each pixel: minimum and maximum allowable fraction images value between −0.05 and 1.05, respectively; shade fraction value lower than 0.8; and, maximum permissible RMSE of 0.025. If several models fulfilled those conditions, the model with the lowest RMSE was chosen. Finally, a shade normalization was performed in the fraction images (GV, NPV and soil) to obtain the relative abundance of non-shade endmembers (Quintano et al., 2017; Roberts et al., 2019) for each sensor. The GV shade normalized fraction corresponds to the FVC.

The Visualization and Image Processing for Environmental Research (VIPER) Tools 2.1 (Roberts et al., 2019) was used to perform the MESMA runtime.

2.5. Field estimation of fractional vegetation cover (FVC) and validation

In summer of 2016 (from June to July) we established 85 plots of 30 × 30 m and 360 plots of 2 × 2 m in the field to evaluate the performance of the FVC estimations made from both the dimidiate pixel model and the multiple endmember spectral mixture analysis for the year 2016 with Landsat OLI and WorldView-2 sensors. The plots were located in the field based on each satellite pixel grid to ensure the alignment between remote sensing and field data using a sub-meter accuracy GPS receiver. The last year of the remote sensing time series after the fire was chosen to validate the FVC estimates since it would exhibit the highest post-fire recovery. We followed a random stratified design, using the surface occupied by the four fire recurrence and severity categories as strata. FVC was measured in each field plot as the percentage of total vegetation cover (i.e. vertical projected area occupied by herbaceous, shrub and pine seedling strata to the total plot extent; Anderson et al., 2005, Calvo et al., 2008; Delamater et al., 2012). Bivariate Pearson correlations and RMSE were computed between the FVC remote sensing estimates and FVC field data.

3. Results

3.1. Estimation of FVC using the dimidiate pixel model

The FVC time series computed from very high spatial resolution WorldView-2 imagery using the dimidiate pixel model showed a substantial decrease after the forest fire disturbance (August 2012)

for each fire recurrence and severity category (Fig. 2). The highest post-fire FVC recovery was found at the categories of high fire recurrence and severity, pre-fire FVC almost being reached four years after fire. Regarding pre-fire conditions, FVC computed from WorldView-2 NDVI (Fig. 2A) was approximately 10% lower than that estimated from RENDVI (Fig. 2B) for the low fire recurrence categories, under a high canopy density.

The FVC time series derived from Landsat using the dimidiate pixel model (Fig. 3) followed almost the same pattern as those obtained from WorldView NDVI at all categories of recurrence and severity. However, for the entire time series, the Landsat derived FVC was slightly lower (between 1 and 20%) than the computed from WorldView-2 NDVI. The difference in the estimated fractional cover was also smaller between fire recurrence and severity categories.

The accuracy of the dimidiate pixel model with regard to the FVC field measurements for the fourth year after the fire was considerably higher for WorldView-2 NDVI and RENDVI based estimates (Fig. 4 and Table 3) than for Landsat OLI NDVI (Fig. 5 and Table 3). The linear relationships assumed for validation purposes were statistically significant at p < 0.001. WorldView-2 RENDVI based estimates predicted FVC with high accuracy for the full range of field-sampled vegetation cover. However, the model based on NDVI calculated from both Landsat OLI and WorldView-2 underestimated FVC at high field-sampled vegetation cover (field-sampled FVC > 80%) (Fig. 4 and Fig. 5).

3.2. Estimation of fractional vegetation cover (FVC) using multiple endmember spectral mixture analysis (MESMA)

Spectral unmixing achieved an average percentage of classified pixels of 93.4% and 91.8% for the WorldView-2 and Landsat imagery time series, respectively. The iterative endmember selection (IES) technique selected nine endmembers which included five photosynthetic vegetation (PV) spectra, two non-photosynthetic vegetation (NPV) spectra and five soil spectra for the WorldView-2 imagery (Table 4). Landsat imagery was unmixed with seven endmembers selected by the IES technique which included four PV spectra, one NPV spectra and three soil spectra (Table 4). See Fig. 6 for an example of the spectral signatures separability of the endmembers grouped in each spectral library.

FVC computed from the photosynthetic vegetation endmember fraction in the MESMA model for WorldView-2 and Landsat imagery (Fig. 7A and B) followed the same temporal pattern as the FVC time series estimated through the dimidiate pixel model. In the MESMA model, however, for low fire recurrence categories and pre-fire conditions, the estimated fraction of photosynthetic vegetation was approximately the same for WorldView-2 and Landsat ETM + .

The linear relationships between field-sampled and estimated FVC values from the MESMA model based on WorldView-2 and Landsat OLI were statistically significant at p < 0.0001. The accuracy of
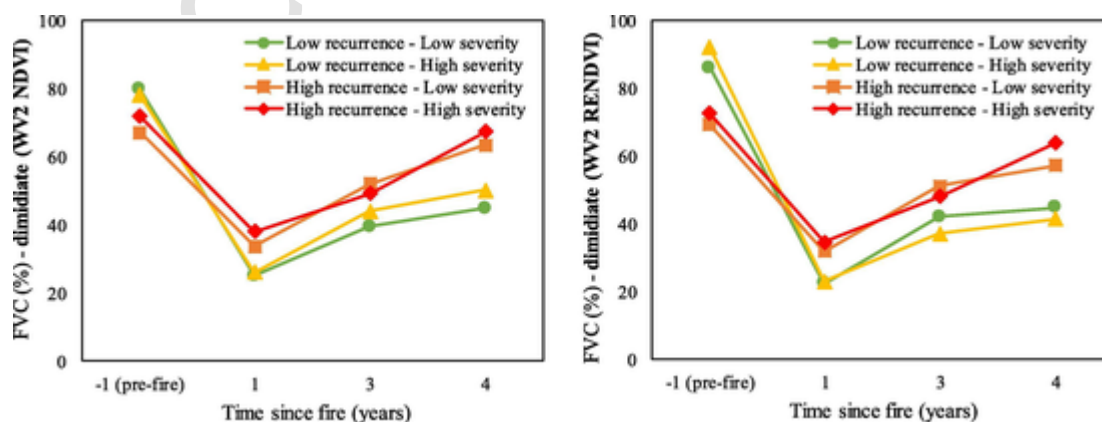

Fig. 2. FVC time series estimated through the dimidiate pixel model from WorldView-2 NDVI (A) and RENDVI (B) in different fire recurrence and severity categories.
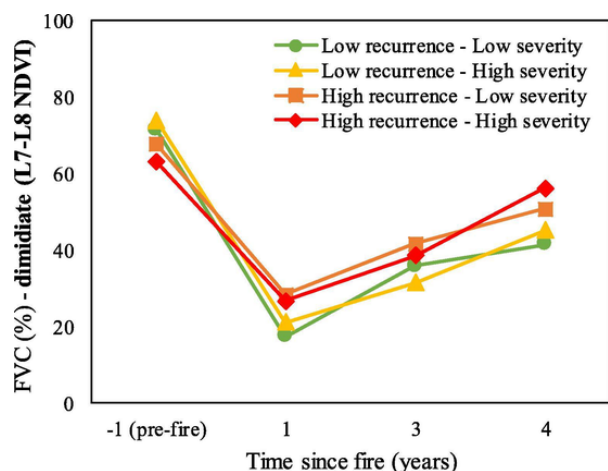
Fig. 3. FVC time series estimated through the dimidiate pixel model from Landsat (ETM + and OLI) NDVI in fire recurrence and severity categories.

the MESMA model was considerably higher than that of the dimidiate pixel model. Although the FVC estimates from MESMA were accurate for the entire range of field-sampled vegetation cover for both sensors, the WorldView-2 derived fraction of photosynthetic vegetation had a higher performance (Fig. 8 and Table 5) than the fraction derived from Landsat OLI (Fig. 9 and Table 5) in terms of R^2 and RMSE.

4. Discussion

FVC is an essential biophysical parameter that allows the quantitative characterization of vegetation communities in the assessment of post-fire forest recovery (Zhang et al., 2013; Meng et al., 2018). Knowledge of post-fire vegetation trajectories considering the fire regime is key for understanding the resilience of communities to present and future disturbances (Yang et al., 2017). Our study demonstrated the potentiality of multi-scale remote sensing techniques to measure post-fire resilience under different fire regime categories. We found that, WorldView-2 satellite imagery outperformed Landsat in the quantitative estimation of FVC in highly heterogeneous landscapes. Additionally, the MESMA model performed better in the vegetation fraction extraction than the dimidiate pixel model based on vegetation indices for the considered remote sensing data. The FVC time series accounting for pre- and post-fire conditions showed the same general pattern in the estimations made at both spatial resolutions and modeling approaches (dimidiate pixel model and MESMA). The categories defined by a high fire recurrence were associated to the highest post-fire recovery, reaching almost pre-fire FVC four years after fire. In these categories, pre-fire vegetation cover was mainly constituted by resprouter shrubs and herbaceous species (Fernández-García et al., 2018b), which show fast post-fire recovery rates and are promoted by recurrent fires (Pausas, 1999; Calvo et al., 2008; Taboada et al., 2017). By contrast, after the occurrence of the stand-replacing fire, the mature pine stand that was present in low fire recurrence scenarios (Fernández-García et al., 2018b) needs more years to reach the cover values observed in pre-fire conditions (Rodrigo et al., 2004). Indeed, looking at the pre-fire conditions in the low recurrence categories, under vigorous pine and oak canopy density, the dimidiate pixel models based on NDVI yielded lower FVC estimates than those based on the red edge NDVI (RENDVI) as spectral response. This result could be related to the saturation effect that vegetation indices computed from red and NIR regions of the electromagnetic spectrum asymptotically reach under dense vegetation with high biomass or leaf area index (Tucker 1977; Mutanga and Skidmore, 2004; Chen et al., 2009). When the ecosystem reaches its biomass production peak, which in our study area occurs in summer (Hedlund et al., 2003), the red light absorbed by the vegetation canopy reaches its maximum level, while NIR reflectance steadily increases because of the multiple scattering

of canopy from dense vegetation (Mutanga et al., 2012; Zhu et al., 2017). The use of spectral indices, such as RENDVI, can overcome the saturation effect (Mutanga et al., 2012) given the higher sensitivity of the red edge region to changes in vegetation biochemical and biophysical parameters (Zhu et al., 2017; Xie et al., 2018), such as chlorophyll content.

The lowest overall FVC values and the smallest differences in FVC between fire recurrence categories, estimated through the dimidiate pixel model using Landsat NDVI, may be caused by a land cover aggregation effect at coarse spatial resolution in our spatially heterogeneous study area. Several studies have highlighted a progressive decrease in NDVI range and mean as less extreme values are detected at coarser spatial resolutions (Stefanov and Netzband, 2005; Sprintsin et al., 2007). For their part, Munyati and Mboweni (2013) found that healthy small vegetation patches presented a decreasing trend in mean NDVI values with increasingly coarser spatial resolution imagery. This effect could have led to an overestimation of the mean Landsat $NDVI_s$ parameter and an underestimation of FVC (Ding et al., 2016). The overall accuracy of the dimidiate pixel model with regard to FVC field measurements using Landsat NDVI as spectral response (10–15% in terms of RMSE) was similar to that achieved in several studies using sensors at moderate or low spatial resolution (Xiao and Moody, 2005; Jiménez-Muñoz et al., 2009; Jiapaer et al., 2011; Zhang et al., 2013). In our study, the use of very high spatial resolution imagery substantially improved the model accuracy (5–10% in terms of RMSE), especially when using RENDVI as spectral signal. Since this spectral index is more sensitive to changes in vegetation biophysical parameters than NDVI and can prevent the saturation effect (Mutanga et al., 2012; Zhu et al., 2017; Xie et al., 2018), FVC was not underestimated at high vegetation cover on pre-fire conditions. Despite this effect, the linear relationship between the FVC estimated from NDVI and the field-sampled FVC was statistically significant, as other studies have found (Jiapaer et al., 2011; Song et al., 2017). Some authors propose methods with high uncertainty (Zeng et al., 2000) to estimate $(RE)NDVI_v$ and $(RE)NDVI_s$ parameters, such as image statistics (maximum and minimum spectral index values over a study area or time series; Gutman and Ignalov, 1998) or averages of vegetation and soil samples of spectral libraries (Jiménez-Muñoz et al., 2009). However, the definition of $(RE)NDVI_v$ and $(RE)NDVI_s$ parameters in this research using high spatial resolution satellite imagery together with field knowledge could avoid the contribution of litter, shadows and other non-interest ground features to the spectral signal of pure vegetation and bare soil training areas (Montandon and Small, 2008; Kouchi et al., 2013; Melville et al., 2019). Despite the good performance obtained with the dimidiate pixel model in estimating FVC from very high spatial resolution satellite imagery, there might be potential constraints to its implementation in more extensive regions than the study area. First, the $(RE)NDVI_s$ parameter could vary substantially among different soil types (Montandon and Small, 2008) because of their mineral composition, organic matter content or moisture (Ding et al., 2016). Thus, in extensive areas with large environmental gradients, soil spectra could exhibit excessive variability to properly characterize it using a single parameter (Xiao and Moody, 2005). The same assumption could be applied for the characterization of vegetation variability with the $(RE)NDVI_v$ parameter over large areas. Indeed, this parameter varies across time and space because of seasonal changes in the vegetation canopy and background soil signal (Mu et al., 2018). Second, the FVC estimation over extensive regions using very high spatial resolution satellite imagery could be constrained due to the high cost per scene of commercial satellite imagery (Nichol et al., 2006; Zhou et al., 2013).

The results obtained in this paper showed that MESMA is an effective approach for monitoring resilience in fire-prone ecosystems (Fernandez-Manso et al., 2016; Meng et al., 2018). The average percentage of classified pixels for WorldView-2 and Landsat imagery was high considering that the same spectral library was used to unmix
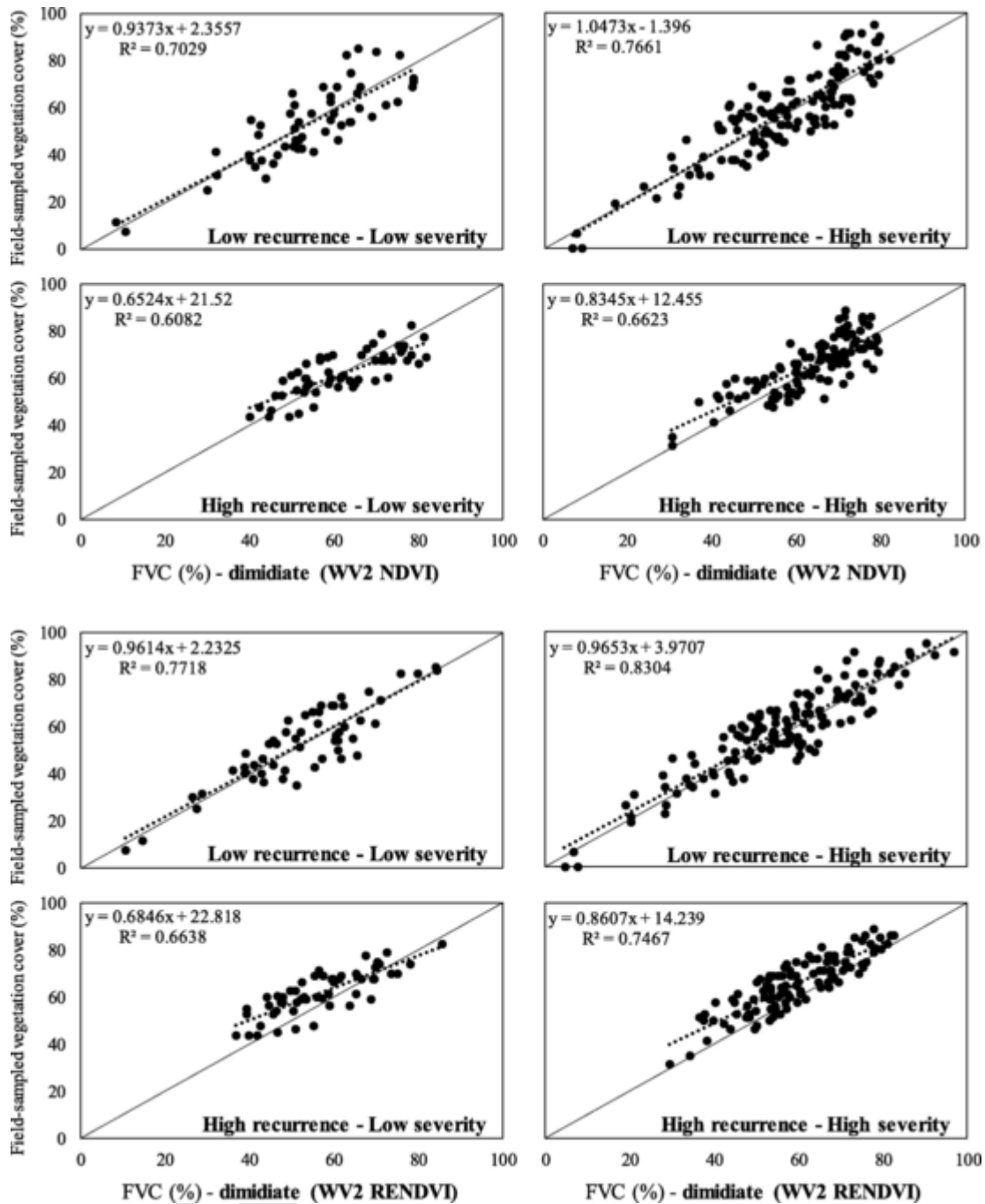
Fig. 4. Relationship between field-sampled and estimated FVC values from the dimidiate pixel model based on WorldView-2 NDVI and RENDVI.

Table 3
Root mean square error (RMSE) values between field-sampled and estimated FVC values from the dimidiate pixel model based on WorldView-2 NDVI/RENDVI and Landsat OLI NDVI.

Dimidiate pixel model	WV2 NDVI	WV2 RENDVI	L-OLI NDVI
Low recurrence - Low severity	9.11	7.91	13.27
Low recurrence - High severity	9.03	7.88	12.61
High recurrence - Low severity	7.00	6.03	11.64
High recurrence - High severity	7.16	6.43	12.32

more than one scene (Fernandez-Manso et al., 2016). The accuracy of MESMA photosynthetic vegetation (PV) fraction estimation with regard to FVC field measurements for Landsat (6–8% in terms of RMSE) and WorldView-2 (4–6% in terms of RMSE) imagery was remarkably higher than that obtained from the dimidiate pixel model. This could be due to the physical meaning of the PV fraction image, which improve its relation with field data (Quintano et al., 2013), and the spectral representability of the selected endmembers (Tane et al., 2018) through the Iterative Endmember Selection (IES) technique. Moreover, in the MESMA model, all available reflectance bands of each sensor are used to unmix the imagery, instead of using two bands as most common spectral indices do (Fernandez-Manso et al., 2016), and the background influence of non-vegetation components is minimized (Xiao and Moody, 2005). Hence, MESMA unmixing could better capture
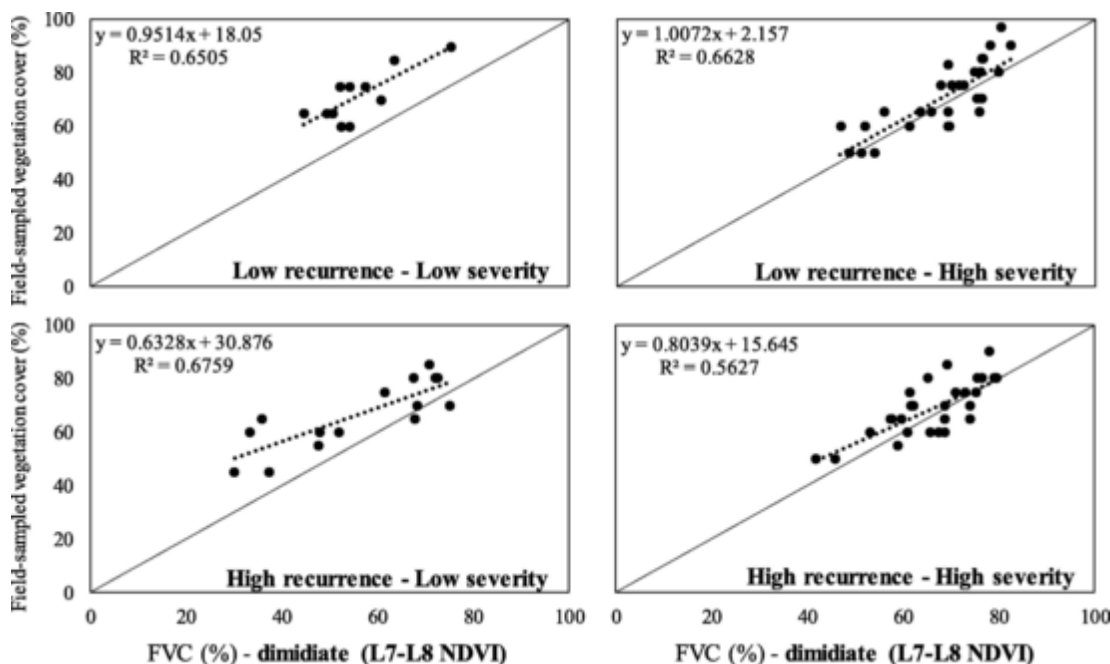
Fig. 5. Relationship between field-sampled and estimated FVC values from the dimidiate pixel model based on Landsat OLI NDVI.

Table 4

Photosynthetic vegetation (PV), non-photosynthetic vegetation (NPV) and soil endmembers selected for the WorldView-2 and Landsat imagery.

PV spectral library	WorldView-2 No. of endmembers	Landsat No. of endmembers
Pinus pinaster	2	2
Quercus sp.	2	1
Shrub	1	1
NPV spectral library		
Woody debris	1	1
Charred logs	1	0
Soil spectral library		
Forest track	1	1
Soil 1	2	1
Soil 2	1	0
Rock	1	1

the ground spectra variability of heterogeneous burned areas than other spectral unmixing methods that use a limited number of endmembers (Xiao and Moody, 2005). In addition, MESMA did not underestimate FVC at high canopy density in pre-fire conditions with any remote sensing data. Twele (2004) also highlighted that the saturation effect observed for vegetation indices based on the red and NIR regions is avoided with spectral mixture analysis techniques. As stated by Tane et al. (2018), a linear relationship was found between the PV fraction and the field-sampled FVC in this study. The overall accuracy of the MESMA modeled fraction of PV for Landsat (6–8% in terms of RMSE) was in line with that reported in previous studies using moderate or low spatial resolution satellite imagery (Powell et al., 2007; Veraverbeke et al., 2012; Okin et al., 2013; Fan and Deng, 2014). PV fraction estimation using WorldView-2 slightly improved the overall model accuracy to an RMSE between 4 and 6%, in every fire recurrence-severity category. The delineation of more spectrally pure endmembers with very high spatial resolution satellite imagery has led to an increase in the accuracy of the unmixing approach (Melville et

al., 2019). The use of remote sensing data at high spatial resolution under a MESMA unmixing approach could be applicable over extensive regions with high environmental gradients as long as the candidate endmembers are properly defined (Quintano et al., 2017). However, it should be assessed whether the slight increase in MESMA model accuracy when using remote sensing data at very high spatial resolution compensates for the higher economic costs of the imagery.

5. Conclusions

1. Our study highlights the strengths and weaknesses of high and moderate spatial resolution satellite imagery for estimating fractional vegetation cover (FCV) in fire-prone pine ecosystems in order to monitor post-fire forest resilience under different fire recurrence and severity categories.
2. In the study area, the highest resilience of vegetation in terms of post-fire FVC recovery corresponds to the high fire recurrence and severity categories.
3. The use of very high spatial resolution satellite imagery to estimate FVC on the basis of the dimidiate pixel model improves model accuracy, particularly when using red edge-NDVI (RENDVI) as spectral signal given the high sensitivity of the red edge region of the spectrum to variability in vegetation biophysical parameters. Moreover, the definition of pure green vegetation and bare soil spectral responses with very high spatial resolution satellite imagery would incorporate small background contributions from non-interest ground features in a heterogeneous landscape.
4. Moderate spatial resolution satellite imagery led to an underestimation of FVC when using the dimidiate pixel model because of a land cover aggregation effect.
5. The physical sense of the MESMA model, together with the minimization of the background influence of non-vegetation components, led to a better characterization of the ground spectra variability than the dimidiate pixel model in a heterogeneous burned area. MESMA improves the accuracy of the vegetation fraction extraction using very high spatial resolution satellite imagery under all considered fire recurrence-severity categories, probably due to the delineation of more spectrally pure endmembers than using coarse resolution remote sensing data.
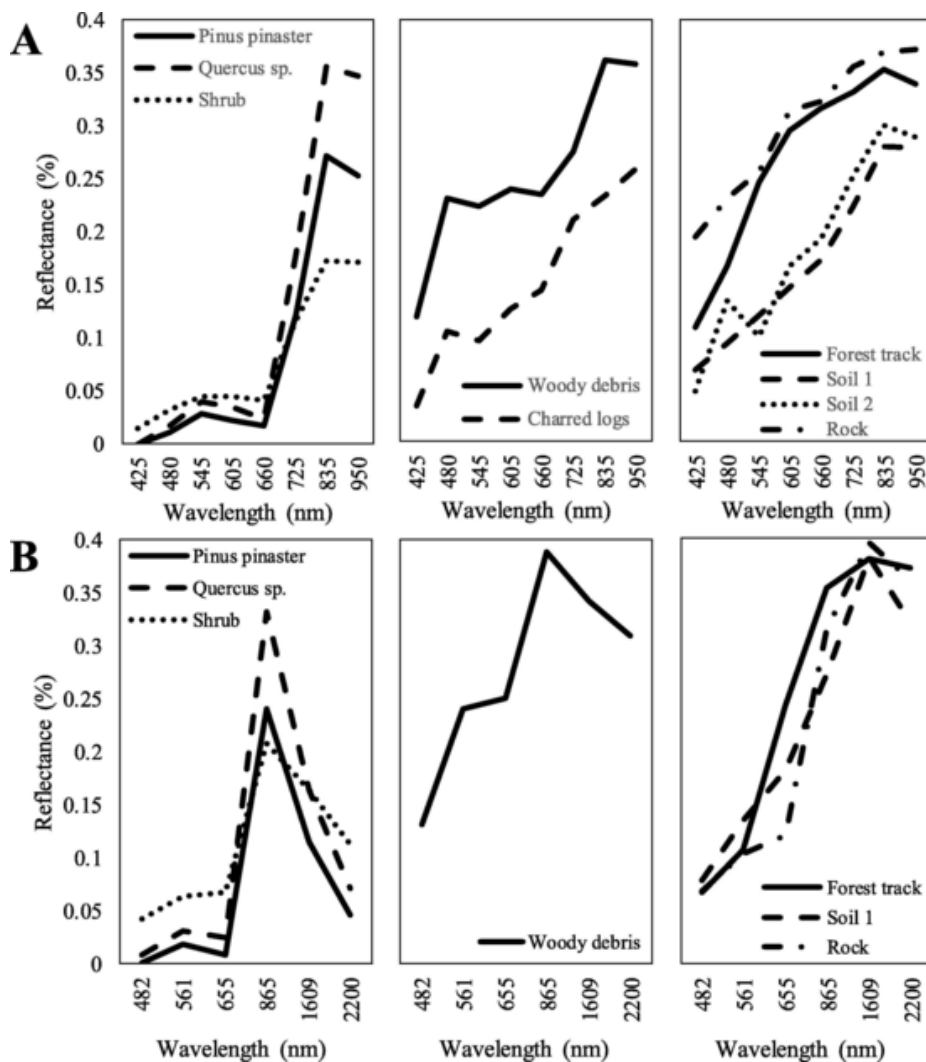
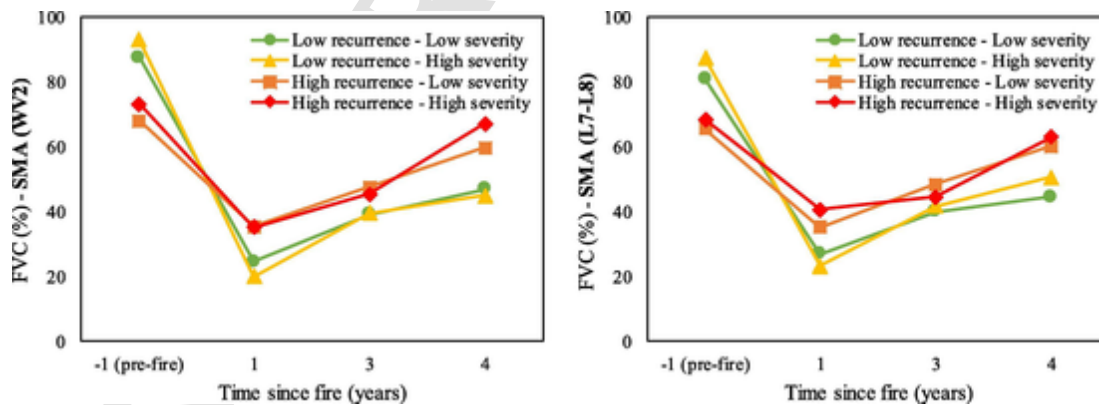**Fig. 6.** Example of WorldView-2 (A) and Landsat (B) endmembers spectra.

Fig. 7. FVC time series estimated through the multiple endmember spectral mixture analysis (MESMA) model from WorldView-2 (A) and Landsat ETM+ and OLI (B) imagery under fire recurrence and severity categories.
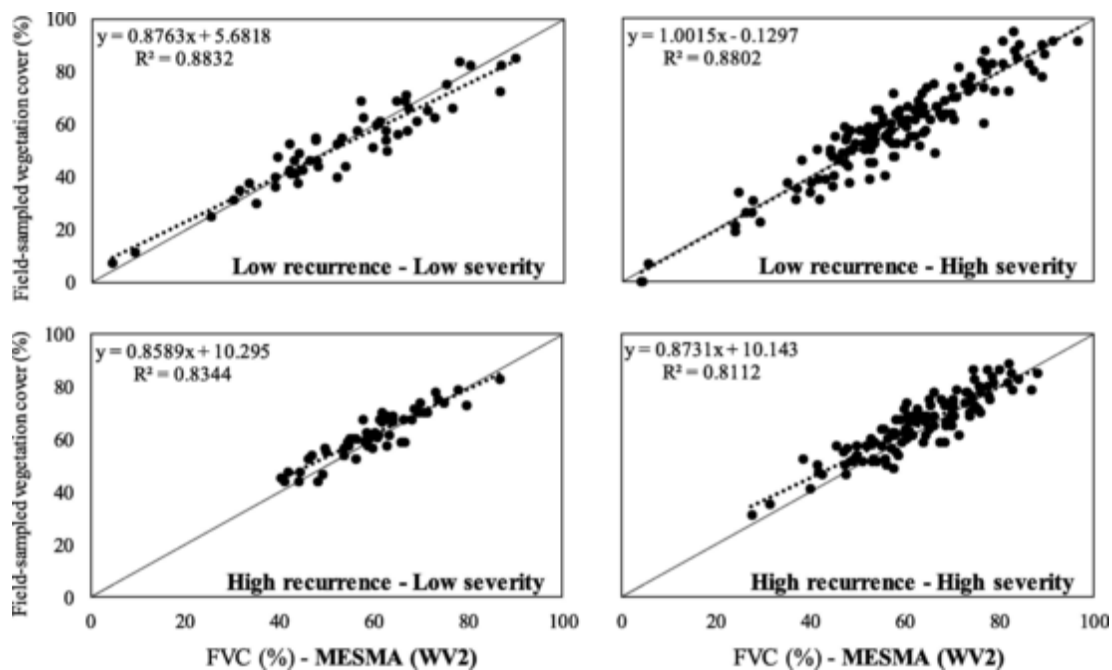
Fig. 8. Relationship between field-sampled and estimated FVC values from the multiple endmember spectral mixture analysis (MESMA) model for WorldView-2.

Table 5

Root mean square error (RMSE) values between field-sampled and estimated FVC values from the multiple endmember spectral mixture analysis (MESMA) model for WorldView-2 and Landsat OLI.

MESMA	WV2	L-OLI
Low recurrence - Low severity	5.1354	7.1546
Low recurrence - High severity	5.3777	7.8885
High recurrence - Low severity	4.4283	6.5495
High recurrence - High severity	5.5957	7.8693

Uncited references

.

Declaration of Competing Interest

The authors declare that they have no known competing financial interests or personal relationships that could have appeared to influence the work reported in this paper.
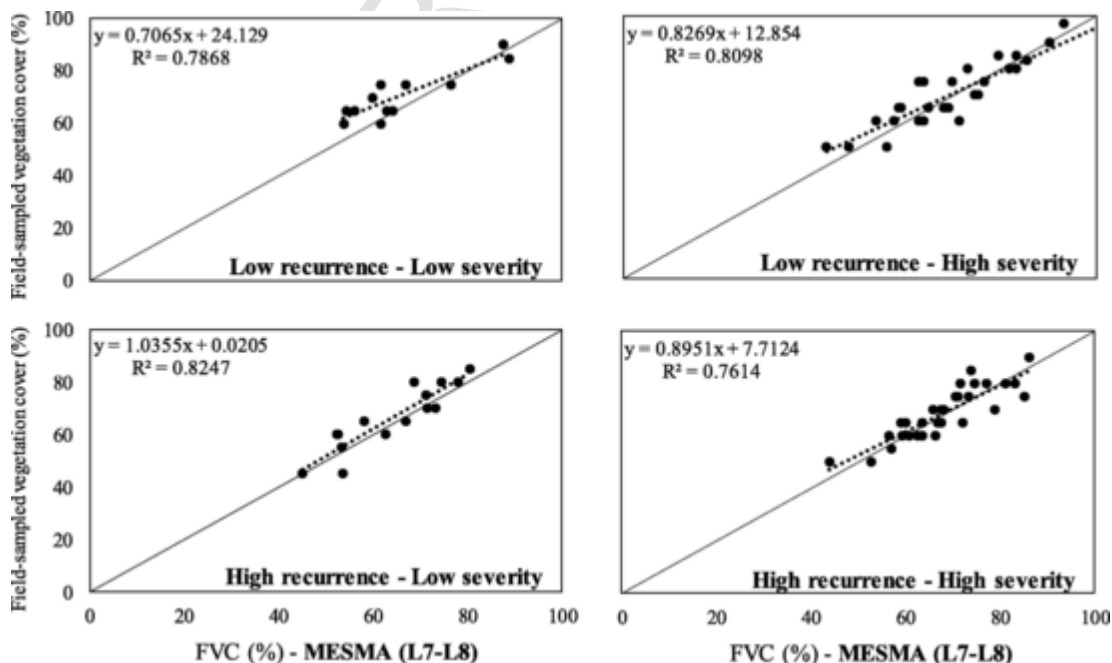

Fig. 9. Relationship between field-sampled and estimated FVC values from the multiple endmember spectral mixture analysis (MESMA) model for Landsat OLI.

Acknowledgments

References

Álvarez, A, Gracia, M, Vayreda, J, Retana, J, 2012. Patterns of fuel types and crown fire potential in Pinus halepensis forest in the Western Mediterranean Basin. For. Ecol. Manage. 270, 282–290.

Anderson, S, Anderson, W, Hines, F, Fountain, A, 2005. Determination of field sampling methods for the assessment of curing levels in grasslands. Bushfire Cooperative Research Centre, Project A1 (4), Report.

Atzberger, C, 2004. Object-based retrieval of biophysical canopy variables using artificial neural nets and radiative transfer models. Remote Sens. Environ. 93, 53–67.

Baret, F, Weiss, M, Lacaze, R, Camacho, F, Makhmara, H, Pacholcyzk, P, Smets, B, 2013. GEOV1: LAI and FAPAR essential climate variables and FCOVER global time series capitalizing over existing products. Part1: Principles of development and production. Remote Sens. Environ. 137, 299–309.

Bian, J, Li, A, Zhang, Z, Zhao, W, Lei, G, Xia, H, Tan, J, 2016. Grassland fractional vegetation cover monitoring using the composited HJ-1A/B time series images and unmanned aerial vehicles: a case study of Zoige wetland, China. In: Proceedings of the IEEE International Geoscience and Remote Sensing Symposium. pp. 7192–7195.

Bue, B D, Thompson, D R, Sellar, R G, Podest, E V, Eastwood, M L, Helmlinger, M C, McCubbin, I B, Morgan, J D, 2015. Leveraging in-scene spectra for vegetation species discrimination with MESMA-MDA. ISPRS J. Photogramm. Remote Sens. 108, 33–48.

Calvo, L, Santalla, S, Valbuena, L, Marcos, E, Tárrega, R, Luis-Calabuig, E, 2008. Post-fire natural regeneration of a Pinus pinaster forest in NW Spain. Plant Ecol. 197, 81–90.

Calvo, L, Hernández, V, Valbuena, L, Taboada, A, 2016. Provenance and seed mass determine seed tolerance to high temperatures associated to forest fires in Pinus pinaster. Annals of Forest Science 73, 381–391.

Carlson, T N, Ripley, D A, 1997. On the relation between NDVI, fractional vegetation cover, and leaf area index. Remote Sens. Environ. 62, 241–252.

Chen, J, Song, G, Shen, M, Tang, Y, Matsushita, B, 2009. Estimating aboveground biomass of grassland having a high canopy cover: an explanatory analysis of in situ hyperspectral data. Int. J. Remote Sens. 24, 6497–6517.

Chu, T, Guo, X, Takeda, K, 2016. Remote sensing approach to detect post-fire vegetation regrowth in Siberian boreal larch forest. Ecol. Ind. 62, 32–46.

Chuvieco, E, Aguado, I, Yebra, M, Nieto, H, Salas, J, Martín, M P, Vilar, L, Martínez, J, Martín, S, Ibarra, P, de la Riva, J, Baeza, J, Rodríguez, F, Molina, J R, Herrera, M A, Zamora, R, 2010. Development of a framework for fire risk assessment using remote sensing and geographic information system technologies. Ecol. Model. 221 (1), 46–58.

Clark, M L, Kilham, N E, 2016. Mapping of land cover in northern California with simulated hyperspectral satellite imagery. ISPRS J. Photogramm. Remote Sens. 119, 228–245.

Cuevas-González, M, Gerard, F, Baltzer, H, Riaño, D, 2009. Analysing forest recovery after wildfire disturbance in boreal Siberia using remotely sensed vegetation indices. Glob. Change Biol. 15, 561–577.

De Santis, A, Chuvieco, E, 2009. GeoCBI: A modified version of the Composite Burn Index for the initial assessment of the short-term burn severity from remotely sensed data. Remote Sens. Environ. 113, 554–562.

De Santis, A, Chuvieco, E, Vaughan, P J, 2009. Short-term assessment of burn severity using the inversion of PROSPECT and GeoSail models. Remote Sens. Environ. 113, 126–136.

DeFries, R S, Townshend, J R G, Hansen, M C, 1999. Continuous fields of vegetation characteristics at the global scale at 1-km resolution. J. Geophys. Res. 104, 16911–16923.

Delamater, P L, Messina, J P, Mark, J K, Cochrane, A, 2012. A hybrid visual estimation method for the collection of ground truth fractional coverage data in a humid tropical environment. Int. J. Appl. Earth Obs. Geoinf. 18, 504–514.

Delegido, J, Verrelst, J, Alonso, L, Moreno, J, 2011. Evaluation of Sentinel-2 Red-Edge Bands for Empirical Estimation of Green LAI and Chlorophyll Content. Sensors 11, 7063–7081.

Díaz-Delgado, R, Lloret, F, Pons, X, Terradas, J, 2002. Satellite evidence of decreasing resilience in Mediterranean plant communities after recurrent wildfires. Ecology 83, 2293–2303.

Ding, Y, Zheng, X, Zhao, K, Xin, X, Liu, H, 2016. Quantifying the Impact of NDVIsoil Determination Methods and NDVIsoil Variability on the Estimation of Fractional Vegetation Cover in Northeast China. Remote Sensing 8, 29.

Doblas-Miranda, E, Alonso, R, Arnan, X, Bermejo, V, Brotons, L, de las Heras, J, Estiarte, M, Hódar, J A, Llorens, P, Lloret, F, López-Serrano, F R, Martínez-Vilalta, J, Moya, D, Peñuelas, J, Pino, J, Rodrigo, A, Roura-Pascual, N, Valladares, F, Vilà, M, Zamora, R, Retana, J, 2017. A review of the combination among global change factors in

forests, shrublands and pastures of the Mediterranean Region: beyond drought effects. Global Planet. Change 148, 42–54.

Dymond, J R, Stephens, P R, Newsome, P F, 1992. Percent vegetation covers of a degrading rangeland from SPOT. Int. J. Remote Sens. 13, 1999–2007.

Elmore, A, Mustard, J, Manning, S, Lobell, D, 2000. Quantifying vegetation change in semiarid environments: precision and accuracy of spectral mixture analysis and the normalized difference vegetation index. Remote Sens. Environ. 73, 87–102.

Fan, F, Deng, Y, 2014. Enhancing endmember selection in multiple endmember spectral mixture analysis (MESMA) for urban impervious surface area mapping using spectral angle and spectral distance parameters. Int. J. Appl. Earth Obs. Geoinf. 33, 290–301.

Fernández-García, V, Santamarta, M, Fernández-Manso, A, Quintano, C, Marcos, E, Calvo, L, 2018. Burn severity metrics in fire-prone pine ecosystems along a climatic gradient using Landsat imagery. Remote Sens. Environ. 206, 205–217.

Fernández-García, V, Quintano, C, Taboada, A, Marcos, E, Calvo, L, Fernández-Manso, A, 2018. Remote Sensing Applied to the Study of Fire Regime Attributes and Their Influence on Post-Fire Greenness Recovery in Pine Ecosystems. Remote Sensing 10, 733.

Fernández-Guisuraga, J M, Calvo, L, Fernández-García, V, Marcos-Porras, E, Taboada, A, Suárez-Seoane, S, 2019. Efficiency of remote sensing tools for post-fire management along a climatic gradient. For. Ecol. Manage. 433, 553–562.

Fernández-Guisuraga, J M, Suárez-Seoane, S, Calvo, L, 2019. Modeling Pinus pinaster forest structure after a large wildfire using remote sensing data at high spatial resolution. For. Ecol. Manage. 446, 257–271.

Fernandez-Manso, A, Quintano, C, Roberts, D A, 2016. Burn severity influence on post-fire vegetation cover resilience from Landsat MESMA fraction images time series in Mediterranean forest ecosystems. Remote Sens. Environ. 184, 112–123.

Fernandez-Manso, A, Quintano, C, Roberts, D A, 2019. Burn severity analysis in Mediterranean forests using maximum entropy model trained with EO-1 Hyperion and LiDAR data. ISPRS J. Photogramm. Remote Sens. 155, 102–118.

Gao, L, Wang, X, Johnson, B A, Tian, Q, Wang, Y, Verrelst, J, Mu, X, Gu, X, 2020. Remote sensing algorithms for estimation of fractional vegetation cover using pure vegetation index values: A review. ISPRS J. Photogramm. Remote Sens. 159, 364–377.

Garrigues, S, Allard, D, Baret, F, Morisette, J, 2008. Multivariate quantification of landscape spatial heterogeneity using variogram models. Remote Sens. Environ. 112, 216–230.

Gitelson, A A, Kaufman, Y J, Stark, R, Rundquist, D, 2002. Novel algorithms for remote estimation of vegetation fraction. Remote Sens. Environ. 80, 76–87.

Gitelson, A A, Viña, A, Ciganda, V, Rundquist, D C, Arkebauer, T J, 2005. Remote estimation of canopy chlorophyll content in crops. Geophys. Res. Lett. 32, L08403.

González-De Vega, S, De las Heras, J, Moya, D, 2016. Resilience of Mediterranean terrestrial ecosystems and fire severity in semiarid areas: Responses of Aleppo pine forests in the short, mid and long term. Sci. Total Environ. 573, 1171–1177.

Graetz, R D, Pech, R R, Davis, A W, 1988. The assessment and monitoring of sparsely vegetated rangelands using calibrated Landsat data. Int. J. Remote Sens. 9, 1201–1222.

Gutman, G, Ignalov, A, 1998. The derivation of the green vegetation fraction from NOAA/AVHRR data for use in numerical weather prediction models. Int. J. Remote Sens. 19, 1533–1543.

Hedlund, K, Regina, I S, Van der Putten, W H, Leps, J, Diaz, T, Korthals, G W, Lavorel, S, Brown, V K, Dagmar, G, Mortimer, S R, Barrueco, C R, Roy, J, Smilauer, P, Smilauerova, M, Van Dijk, C, 2003. Plant species diversity, plant biomass and responses of the soil community on abandoned land across Europe: idiosyncracy or above-belowground time lags. Oikos 103, 45–58.

Hill, M J, Zhou, Q, Sun, Q, Schaaf, C B, Palace, M, 2017. Relationships between vegetation indices, fractional cover retrievals and the structure and composition of Brazilian Cerrado natural vegetation. Int. J. Remote Sens. 38, 874–905.

Huemmrich, K F, 2001. The GeoSail model: a simple addition to the SAIL model to describe discontinuous canopy reflectance. Remote Sens. Environ. 75, 423–431.

Jacquemoud, S, Baret, F, 1990. PROSPECT: a model of leaf optical properties spectra. Remote Sens. Environ. 34, 75–91.

Jacquemoud, S, Verhoef, W, Baret, F, Bacour, C, Zarco-Tejada, P J, Asner, G P, François, C, Ustin, S L, 2009. PROSPECT + SAIL models: a review of use for vegetation characterization. Remote Sens. Environ. 113, 56–66.

Jia, K, Liang, S, Liu, S, Li, Y, Xiao, Z, Yao, Y, Jiang, B, Zhao, X, Wang, X, Xu, S, Cui, J, 2015. Global Land Surface Fractional Vegetation Cover Estimation Using General Regression Neural Networks from MODIS Surface Reflectance. IEEE Trans. Geosci. Remote Sens. 53, 4787–4796.

Jia, K, Liang, S, Gu, X, Baret, F, Wei, X, Wang, X, Yao, Y, Yang, L, Li, Y, 2016. Fractional vegetation cover estimation algorithm for Chinese GF-1 wide field view data. Remote Sens. Environ. 177, 184–191.

Jiang, Z, Huete, A R, Chen, J, Chen, Y, Li, J, Yan, G, Zhang, X, 2006. Analysis of NDVI and scaled difference vegetation index retrievals of vegetation fraction. Remote Sens. Environ. 101, 366–378.

Jiapaer, G, Chen, X, Bao, A, 2011. A comparison of methods for estimating fractional vegetation cover in arid regions. Agric. For. Meteorol. 151, 1698–1710.

Jiménez-Muñoz, J C, Sobrino, J A, Plaza, A, Guanter, L, Moreno, J, Martinez, P, 2009. Comparison Between Fractional Vegetation Cover Retrievals from Vegetation Indices and Spectral Mixture Analysis: Case Study of PROBA/CHRIS Data Over an Agricultural Area. Sensors 9, 768–793.

Jing, X, Yao, W, Wang, J, Song, X, 2010. A study on the relationship between dynamic change of vegetation Coverage and precipitation in Beijing's mountainous areas during the last 20 years. Math. Comput. Modell. 54, 1079–1085.

Johnson, B, Tateishi, R, Kobayashi, T, 2012. Remote Sensing of Fractional Green Vegetation Cover Using Spatially-Interpolated Endmembers. Remote Sensing 4, 2619–2634.

Jurdao, S, Yebra, M, Guerschman, J P, Chuvieco, E, 2013. Regional estimation of woodland moisture content by inverting Radiative Transfer Models. Remote Sens. Environ. 132, 59–70.

Kallel, A, Le Hégarat-Mascle, S, Ottlé, C, Hubert-Moy, L, 2007. Determination of vegetation cover fraction by inversion of a four-parameter model based on isoline parametrization. Remote Sens. Environ. 111, 553–566.

Kattenborn, T, Schmidtlein, S, 2019. Radiative transfer modelling reveals why canopy reflectance follows function. Sci. Rep. 9, 6541.

Key, C H, 2006. Ecological and sampling constraints on defining landscape fire severity. Fire Ecology 2, 34–59.

Key, C.H., Benson, N.C., 2006. Landscape assessment (LA) sampling and analysis methods. USDA Forest Service general technical report (RMRS-GTR-164-CD).

Kötz, B, Schaepman, M, Morsdorf, F, Bowyer, P, Itten, K, Allgöwer, B, 2004. Radiative transfer modeling within a heterogeneous canopy for estimation of forest fire fuel properties. Remote Sens. Environ. 92, 332–344.

Kouchi, H.S., Sahebi, M.R., Abkar, A.A. and Zoej, M.J.V., 2013. Fractional Vegetation Cover Estimation in Urban Environments. International Archives of the Photogrammetry, Remote Sensing and Spatial Information Sciences, vol. XL-1/W3, pp. 357–360.

Li, W, Weiss, M, Waldner, F, Defourny, P, Demarez, V, Morin, D, Hagolle, O, Baret, F A, 2015. Generic Algorithm to Estimate LAI, FAPAR and FCOVER Variables from SPOT4_HRVIR and Landsat Sensors: Evaluation of the Consistency and Comparison with Ground Measurements. Remote Sensing 7, 15494–15516.

Li, Y, Wang, H, Li, X B, 2015. Fractional Vegetation Cover Estimation Based on an Improved Selective Endmember Spectral Mixture Model. PLoS ONE 10 (4), e0124608.

Liang, Z, Bing-fang, W, Yue-min, Z, Ji-hua, M, Ning, Z, 2008. A study of fast estimation of vegetation fraction in Three Gorges emigration area by using SPOT5 imagery. Int. Arch. Photogramm. Remote Sens. Spat. Inform. Sci. 37, 987–992.

Melville, B, Fisher, A, Lucieer, A, 2019. Ultra-high spatial resolution fractional vegetation cover from unmanned aerial multispectral imagery. Int. J. Appl. Earth Obs. Geoinf. 78, 14–24.

Meng, R, Wu, J, Schwager, K L, Zhao, F, Dennison, P E, Cook, B D, Brewster, K, Green, T M, Serbin, S P, 2017. Using high spatial resolution satellite imagery to map forest burn severity across spatial scales in a Pine Barrens ecosystem. Remote Sens. Environ. 191, 95–109.

Meng, R, Wu, J, Zhao, F, Cook, B D, Hanavan, R P, Serbin, S P, 2018. Measuring short-term post-fire forest recovery across a burn severity gradient in a mixed pine-oak forest using multi-sensor remote sensing techniques. Remote Sens. Environ. 210, 282–296.

Montandon, L M, Small, E E, 2008. The impact of soil reflectance on the quantification of the green vegetation fraction from NDVI. Remote Sens. Environ. 112, 1835–1845.

Mu, X, Song, W, Gao, Z, McVicar, T R, Donohue, R J, Yan, G, 2018. Fractional vegetation cover estimation by using multi-angle vegetation index. Remote Sens. Environ. 216, 44–56.

Munyati, C, Mboweni, G, 2013. Variation in NDVI values with change in spatial resolution for semi-arid savanna vegetation: a case study in northwestern South Africa. Int. J. Remote Sens. 34, 2253–2267.

Mutanga, O, Skidmore, A K, 2004. Narrow band vegetation indices overcome the saturation problem in biomass estimation. Int. J. Remote Sens. 25, 3999–4014.

Mutanga, O, Adam, E, Cho, M A, 2012. High density biomass estimation for wetland vegetation using WorldView-2 imagery and random forest regression algorithm. Int. J. Appl. Earth Obs. Geoinf. 18, 399–406.

Nichol, J E, Shaker, A, Wong, M-S, 2006. Application of high-resolution stereo satellite images to detailed landslide hazard assessment. Geomorphology 76, 68–75.

Ninyerola, M., Pons, X., Roure, J.M., 2005. Atlas Climático Digital de la Península Ibérica. Metodología y aplicaciones en bioclimatología y geobotánica. Universidad Autónoma de Barcelona.

North, P R J, 2002. Estimation of fAPAR, LAI, and vegetation fractional cover from ATSR-2 imagery. Remote Sens. Environ. 80, 114–121.

Okin, G S, Clarke, K D, Lewis, M M, 2013. Comparison of methods for estimation of absolute vegetation and soil fractional cover using MODIS normalized BRDF-adjusted reflectance data. Remote Sens. Environ. 130, 266–279.

Pausas, J G, 1999. Response of plant functional types to changes in the fire regime in Mediterranean ecosystems: A simulation approach. J. Veg. Sci. 10, 717–722.

Pausas, J G, Fernández-Muñoz, S, 2012. Fire regime changes in the Western Mediterranean Basin: from fuel-limited to drought-driven fire regime. Clim. Change 110, 215–226.

Pausas, J G, Keeley, J E, 2014. Evolutionary ecology of resprouting and seeding in fire-prone ecosystems. New Phytol. 204, 55–65.

Powell, R L, Roberts, D A, Dennison, P E, Hess, L L, 2007. Sub-pixel mapping of urban land cover using multiple endmember spectral mixture analysis: Manaus, Brazil. Remote Sens. Environ. 106, 253–267.

Purevdor, J T S, Tateishi, R, Ishiyama, T, 1998. Relationships between percent vegetation cover and vegetation indices. Int. J. Remote Sens. 19, 3519–3535.

Quintano, C, Fernández-Manso, A, Calvo, L, Marcos, E, Valbuena, L, 2015. Land surface temperature as potential indicator of burn severity in forest Mediterranean ecosystems. Int. J. Appl. Earth Obs. Geoinf. 36, 1–12.

Quintano, C, Fernández-Manso, A, Roberts, D A, 2013. Multiple Endmember Spectral Mixture Analysis (MESMA) to map burn severity levels from Landsat images in Mediterranean countries. Remote Sens. Environ. 136, 76–88.

Quintano, C, Fernandez-Manso, A, Roberts, D A, 2017. Burn severity mapping from Landsat MESMA fraction images and Land Surface Temperature. Remote Sens. Environ. 190, 83–95.

Richter, R., Schläpfer, D., 2018. Atmospheric/Topographic Correction for Satellite Imagery. DLR report (DLR-IB 565-01/2018).

Roberts, D A, Dennison, P E, Gardner, M, Hetzel, Y, Ustin, S L, Lee, C, 2003. Evaluation of the potential of hyperion for fire danger assessment by comparison to the airborne visible/infrared imaging spectrometer. IEEE Trans. Geosci. Remote Sens. 41, 1297–1310.

Roberts, D A, Gardner, M, Church, R, Ustin, S, Scheer, G, Green, R O, 1998. Mapping Chaparral in the Santa Monica Mountains Using Multiple Endmember Spectral Mixture Models. Remote Sens. Environ. 65, 267–279.

Roberts, D A, Quattrochi, D A, Hulley, G C, Hook, S J, Green, R O, 2012. Synergies between VSWIR and TIR data for the urban environment: an evaluation of the potential for the hyperspectral infrared imager (HyspIRI) decadal survey mission. Remote Sens. Environ. 117, 83–101.

Roberts, D.A., Halligan, K., Dennison, P., Dudley, K., Somers, B., Crabbe, A., 2019. Viper Tools User Manal, Version 2.1, pp. 92.

Rodrigo, A, Retana, J, Picó, F X, 2004. Direct regeneration is not the only response of Mediterranean forests to large fires. Ecology 85, 716–729.

Roth, K L, Dennison, P E, Roberts, D A, 2012. Comparing endmember selection techniques for accurate mapping of plant species and land cover using imaging spectrometer data. Remote Sens. Environ. 127, 139–152.

Roy, D P, Kovalskyy, V, Zhang, H K, Vermote, E F, Yan, L, Kumar, S S, Egorov, A, 2016. Characterization of Landsat-7 to Landsat-8 reflective wavelength and normalized difference vegetation index continuity. Remote Sens. Environ. 185, 57–70.

Sankey, T, Moffet, C, Weber, K, 2008. Postfire recovery of sagebrush communities: assessment using SPOT-5 and very large-scale aerial imagery. Rangeland Ecol. Manage. 61, 598–604.

Scanlon, T M, Albertson, J D, Caylor, K K, Williams, C A, 2002. Determining land surface fractional cover from NDVI and rainfall time series for a savanna ecosystem. Remote Sens. Environ. 82, 376–388.

Schaaf, A N, Dennison, P E, Fryer, G K, Roth, K L, Roberts, D A, 2011. Mapping plant functional types at multiple spatial resolutions using imaging spectrometer data. GIScience and Remote Sensing 48, 324–344.

Sinha, S K, Padalia, H, Dasgupta, A, Verrelst, J, Rivera, J P, 2020. Estimation of leaf area index using PROSAIL based LUT inversion, MLRA-GPR and empirical models: Case study of tropical deciduous forest plantation, North India. Int. J. Appl. Earth Obs. Geoinf. 86, 102027.

Solans-Vila, J P, Barbosa, P, 2010. Post-fire vegetation regrowth detection in the Deiva Marina region (Liguria-Italy) using Landsat TM and ETM+ data. Ecol. Model. 221, 75–84.

Song, W, Mu, X, Ruan, G, Gao, Z, Li, L, Yan, G, 2017. Estimating fractional vegetation cover and the vegetation index of bare soil and highly dense vegetation with a physically based method. Int. J. Appl. Earth Obs. Geoinf. 58, 168–176.

Sprintsin, M, Karnieli, A, Berliner, P, Rotenberg, E, Yakir, D, Cohen, S, 2007. The effect of spatial resolution on the accuracy of leaf area index estimation for a forest planted in the desert transition zone. Remote Sens. Environ. 109, 416–428.

Stefanov, W L, Netzband, M, 2005. Assessment of ASTER land cover and MODIS NDVI data at multiple scales for ecological characterization of an arid urban center. Remote Sens. Environ. 99, 31–43.

Taboada, A, Tárrega, R, Marcos, E, Valbuena, L, Suárez-Seoane, S, Calvo, Leonor, 2017. Fire recurrence and emergency post-fire management influence seedling recruitment and growth by altering plant interactions in fire-prone ecosystems. For. Ecol. Manage. 402, 63–75.

Taboada, A, Fernández-García, V, Marcos, E, Calvo, L, 2018. Interactions between large high-severity fires and salvage logging on a short return interval reduce the regrowth of fire-prone serotinous forests. For. Ecol. Manage. 414, 54–63.

Tane, Z, Roberts, D, Veraverbeke, S, Casas, Á, Ramirez, C, Ustin, S, 2018. Evaluating Endmember and Band Selection Techniques for Multiple Endmember Spectral Mixture Analysis using Post-Fire Imaging Spectroscopy. Remote Sensing 10, 389.

Tessler, N, Wittenberg, L, Provizor, E, Greenbaum, N, 2014. The influence of short-interval recurrent forest fires on the abundance of Aleppo pine (Pinus halepensis Mill.) on Mount Carmel, Israel. Forest Ecol. Manage. 324, 109–116.

Tucker, C J, 1977. Asymptotic nature of grass canopy spectral reflectance. Appl. Opt. 16, 1151–1156.

Twele, A., 2004. Post-Fire Vegetation Regeneration. The Case Study of the "Massif de l'Etoile" Fire. EUR - Scientific and Technical Research Reports (EUR 21010 EN).

Veraverbeke, S, Somers, B, Gitas, I, Katagis, T, Polychronaki, A, Goossens, R, 2012. Spectral mixture analysis to assess post-fire vegetation regeneration using Landsat Thematic Mapper imagery: Accounting for soil brightness variation. Int. J. Appl. Earth Obs. Geoinf. 14, 1–11.

Verger, A, Baret, F, Camacho, F, 2011. Optimal modalities for radiative transfer-neural network estimation of canopy biophysical characteristics: Evaluation over an agricultural area with CHRIS/PROBA observations. Remote Sens. Environ. 115, 415–426.

Verrelst, J, Sabater, N, Rivera, J P, Muñoz-Marí, J, Vicent, J, Camps-Valls, G, Moreno, J, 2016. Emulation of Leaf, Canopy and Atmosphere Radiative Transfer Models for Fast Global Sensitivity Analysis. Remote Sensing 8, 673.

Vilà-Cabrera, A, Coll, L, Martínez-Vilalta, J, Retana, J, 2018. Forest management for adaptation to climate change in the Mediterranean basin: A synthesis of evidence. For. Ecol. Manage. 407, 16–22.

Wang, X, Jia, K, Liang, S, Li, Q, Wei, X, Yao, Y, Zhang, X, Tu, Y, 2017. Estimating Fractional Vegetation Cover from Landsat-7 ETM+ Reflectance Data Based on a Coupled Radiative Transfer and Crop Growth Model. IEEE Trans. Geosci. Remote Sens. 55, 5539–5546.

Wei, X, Wang, S, Wang, Y, 2018. Spatial and temporal change of fractional vegetation cover in North-western China from 2000 to 2010. Geol. J. 53, 427–434.

White, M A, Asner, G P, Nemani, R R, Privette, J L, Running, S W, 2000. Measuring Fractional Cover and Leaf Area Index in Arid Ecosystems: Digital Camera, Radiation Transmittance, and Laser Altimetry Methods. Remote Sens. Environ. 74, 45–57.

Wittich, K P, Hansing, O, 1995. Area-averaged vegetative cover fraction estimated from satellite data. Int. J. Biometeorol. 38, 209–215.

Wu, B, Li, M, Yan, C, Zhou, W, 2004. Developing method of vegetation fraction estimation by remote sensing for soil loss equation: A case in the upper basin of Miyun Reservoir. In: Proceedings of the IEEE International Geoscience and Remote Sensing Symposium. pp. 4352–4355.

Xiao, J, Moody, A, 2005. A comparison of methods for estimating fractional green vegetation cover within a desert-to-upland transition zone in central New Mexico, USA. Remote Sens. Environ. 98, 237–250.

Xie, Q, Dash, J, Huang, W, Peng, D, Qin, Q, Mortimer, H, Casa, R, Pignatti, S, Laneve, G, Pascucci, S, Dong, Y, Ye, H, 2018. Vegetation Indices Combining the Red and Red-Edge Spectral Information for Leaf Area Index Retrieval. IEEE J. Sel. Top. Appl. Earth Obs. Remote Sens. 11, 1482–1493.

Yang, G, Pu, R, Zhang, J, Zhao, C, Feng, H, Wang, J, 2013. Remote sensing of seasonal variability of fractional vegetation cover and its object-based spatial pattern analysis over mountain areas. ISPRS J. Photogramm. Remote Sens. 77, 79–93.

Yang, L, Jia, K, Liang, S, Liu, J, Wang, X, 2016. Comparison of Four Machine Learning Methods for Generating the GLASS Fractional Vegetation Cover Product from MODIS Data. Remote Sensing 8, 682.

Yang, J, Pan, S, Dangal, S, Zhang, B, Wang, S, Tian, H, 2017. Continental-scale quantification of post-fire vegetation greenness recovery in temperate and boreal North America. Remote Sens. Environ. 199, 277–290.

Yebra, M, Chuvieco, E, 2009. Linking ecological information and radiative transfer models to estimate fuel moisture content in the Mediterranean region of Spain: Solving the ill-posed inverse problem. Remote Sens. Environ. 113, 2403–2411.

Zeng, X, Dickinson, R E, Walker, A, Shaikh, M, DeFries, R S, Qi, J, 2000. Derivation and evaluation of global 1 km fractional vegetation cover data for land modeling. J. Appl. Meteorol. Climatol. 39, 826–839.

Zhang, X, Liao, C, Li, J, Sun, Q, 2013. Fractional vegetation cover estimation in arid and semi-arid environments using HJ-1 satellite hyperspectral data. Int. J. Appl. Earth Obs. Geoinf. 21, 506–512.

Zhou, Q, Robson, M, 2001. Automated rangeland vegetation cover and density estimation using ground digital images and a spectral-contextual classifier. Int. J. Remote Sens. 22, 3457–3470.

Zhou, J, Proisy, C, Descombes, X, le Maire, G, Nouvellon, Y, Stape, J L, Viennois, G, Zerubia, J, Couteron, P, 2013. Mapping local density of young Eucalyptus plantations by individual tree detection in high spatial resolution satellite images. For. Ecol. Manage. 301, 129–141.

Zhu, Y, Liu, K, Liu, L, Myint, S W, Wang, S, Liu, H, He, Z, 2017. Exploring the Potential of WorldView-2 Red-Edge Band-Based Vegetation Indices for Estimation of Mangrove Leaf Area Index with Machine Learning Algorithms. Remote Sensing 9, 1060.